Integrating Mechanochemical Synthesis of a Pyridinium-Based Graphitic Ionic Framework into an Eco-Friendly Gold Recycling Process

Zhi-Wei Liu,[a,b] Zhizhuo Yang,[b] Zhaoying Zhang,[a] Xilin Gao,[b] Chuanying Liu,*[a,b] Chengliang Xiao*[a,b]

[a] College of Chemical and Biological Engineering, Zhejiang University, Hangzhou 310058, China.

[b] Institute of Zhejiang University-Quzhou, Quzhou 324000, China

E-mail: xiaoc@zju.edu.cn; cyliu@zju.edu.cn

Materials and reagents

Cyanuric chloride was purchased from Aldrich Sigma. Thiourea, N-bromosuccinimide, 2,4,6-tripyridin-4-yl-1,3,5-triazine, and solvents were purchased from Adamas-beta. Sodium Tetrachloroaurate(III) ($NaAuCl_4$, 99% purity, Yuanye Regeant, Shanghai). All organic solvents are of anhydrous grade and used without further purification.

Instruments and Characterization

Elemental analysis was performed using an Elementar Unicube elemental analyzer. Thermogravimetric analysis (TGA) was conducted on a Mettler-Toledo DSC 3 instrument with a heating rate of 10°C/min under a nitrogen atmosphere. Fourier-transform infrared spectroscopy (FTIR) measurements were carried out on a Bruker INVENIO R spectrometer. Gas adsorption analysis was performed using a Micromeritics 3FLEX instrument, with samples degassed at 80°C for 12 h before measurement. Solid-state nuclear magnetic resonance (NMR) spectroscopy was performed on a Bruker AVANCE NEO 600WB spectrometer operating at 600.41 MHz for 1 hour and 150.98 MHz for ^{13}C, equipped with a 3.2 mm probe. The ^{13}C cross-polarization with total suppression of spinning sidebands (CPTOSS) experiment was conducted at a magic angle spinning (MAS) rate of 10 kHz, with a recycle delay of 5 s and 720 scans. Chemical shifts were referenced to adamantane at 38.5 ppm. Field-emission scanning electron microscopy (FE-SEM) was conducted using a Hitachi

Regulus 8230 instrument equipped with an Oxford energy-dispersive X-ray spectroscopy (EDX) detector, with samples sputter-coated using an MC1000 gold coater. High-resolution transmission electron microscopy (HR-TEM) was performed on an FEI Talos F200X instrument, with samples prepared by dispersing the particles in anhydrous tetrahydrofuran (THF) via ultrasonication and depositing onto ultrathin copper grids. X-ray photoelectron spectroscopy (XPS) was conducted using a Kratos AXIS Supra$^+$ spectrometer. X-ray diffraction (XRD) measurements were performed on a Rigaku Ultima IV diffractometer equipped with a Cu Kα_1 radiation source (λ = 1.5406 Å). Data were collected in the 2θ range of 5–60° with a scanning rate of 5° min^{-1} under ambient conditions.

Equipment for the ball milling process

Ball milling was conducted in a YXQM-0.4L planetary ball mill (Miqi Technology, Changsha, China). The ball milling jars are made of polytetrafluoroethylene (PTFE). The grinding balls are composed of agate with 8.0-mm diameters. The ball milling process is conducted at room temperature in air, while the loading process is carried out in a glove box. The ball milling jars are sealed with tape and tightly compressed to minimize air ingress.

Mechanochemical synthesis of GIF-4 in the planetary mill

The synthesis was performed in a planetary ball mill using four PTFE jars operated in parallel. Each jar was charged with TCT (0.50 g, 2.71 mmol) and TPT (0.93 g, 2.98 mmol). The mixture was milled for 2 h, after which the crude product was washed with anhydrous THF and subsequently purified by Soxhlet extraction (THF) for 24 h. The process afforded the target product in 64.8 % isolated yield, corresponding to a total product mass of 3.51 g per batch.

To quantitatively assess the production efficiency of the mechanochemical synthesis, the space-time yield (STY) was calculated as a key metric for evaluating scalability and process intensification. The STY, defined as the mass of product obtained per unit reactor volume per unit time, was determined based on the following equation:

$$\mathrm{STY} = m_\mathrm{p} / (V_\mathrm{e} \times t) \tag{6}$$

Where STY is the space–time yield (g·L^{-1}·h^{-1}), m is the total mass of product obtained per batch (g), Ve is the total effective reactor volume (L), t is the reaction time (h).

Gold adsorption isotherms with GIF-4

The adsorption isotherms were investigated as follows: 10 mg of the GIF-4 material were added to a set of solutions with varying volumes (5, 6, 8, 10, 12, 14, and 15 mL) of a gold solution with an initial concentration of 1000 ppm (pH = 3.4). The suspensions were then stirred at room temperature for 12 h to ensure the adsorption equilibrium was reached. After the equilibration period, the mixtures were centrifuged to separate the solid adsorbent from the liquid phase. The supernatant was subsequently filtered through a 0.22 μm membrane filter. The concentration of Au(III) was determined by ICP-OES.

The adsorption capacity at equilibrium Q_e (mg/g), was calculated using the following equation:

$$Q_e=(C_0-C_e)\,V/m \tag{1}$$

Where C_0 is the initial concentration of Au (ppm), C_e is the equilibrium concentration, V is the volume of the solution (L), m is the mass of the adsorbent GIF-4 (g). The equilibrium adsorption capacity Q_e versus the equilibrium concentration C_e was fitted with the Langmuir and the Freundlich isotherm models.

Gold adsorption kinetics with GIF-4

A precisely weighed mass (50 mg) of GIF-4 was introduced into a 50 mL aliquot of 20 ppm Au(III) solution ($NaAuCl_4$). The resulting suspension was agitated at room temperature and 150 rpm. At predetermined time intervals (0.5–30 min), 1.0 mL aliquots of supernatant were withdrawn, diluted five-fold with deionized water, and filtered through a 0.22 μm syringe filter. The remaining Au(III) concentration (C_t) in the filtrate was then determined by ICP-OES. The removal efficiency (*RE*) is calculated based on the following equation:

$$RE = \frac{C_0 - C_t}{C_0} \times 100\% \tag{2}$$

where C_0 (mg L^{-1}) is the initial concentration, C_t (mg L^{-1}) is the concentration at the desired time. The experiments were replicated three times.

Langmuir Isotherm Model

The Langmuir model assumes monolayer adsorption onto a surface with a finite number

of active sites. It is expressed by the following equation,

$$Q_e = Q_m K_L C_e / (1+K_L C_e) \quad (3)$$

The linear equation is expressed as follows,

$$\frac{C_e}{Q_e} = \frac{C_e}{Q_m} + \frac{1}{K_L Q_m} \quad (4)$$

where Q_m is the maximum adsorption capacity (mg g^{-1}), K_L is the Langmuir constant related to the affinity of binding sites (L mg^{-1}).

Freundlich isotherm model

The Freundlich model is an empirical equation for heterogeneous surfaces and multilayer adsorption. It is expressed by the following equation,

$$Q_e = K_F C_e^{1/n} \quad (5)$$

The linear form of the Freundlich equation is expressed as follows,

$$\ln Q_e = \ln K_F + \frac{1}{n} \ln C_e \quad (6)$$

where K_F is the Freundlich constant indicative of the adsorption capacity ((mg/g)/$(mg/L)^{1/n}$), 1/n is the heterogeneity factor, an empirical constant related to adsorption intensity.

Kinetic models fitting.

Linear forms of Lagergren pseudo-first-order and pseudo-second-order kinetic models were applied here. The first-order linear equation is expressed as follows.

$$\ln(Q_e - Q_t) = \ln Q_e - k_1 t \quad (7)$$

The second-order linear equation is expressed as follows.

$$\frac{t}{Q_t} = \frac{1}{k_2 Q_e^2} + \frac{t}{Q_e} \quad (8)$$

where Q_e and Qt are the adsorption amount (mg g^{-1}) at equilibrium and time t (min), respectively, k_1 is the rate constant (min^{-1}) of the pseudo-first-order kinetics model, and k_2 is the rate constant (g (mg min)$^{-1}$) of the pseudo-second-order kinetics model. The plots of $\ln(Q_e - Q_t)$ versus t for the pseudo-first-order equation and t/Q_t versus t for the pseudo-second-order equation were tried.

Adsorption with $[AuBr]_4^-$ as the adsorbate.

The experimental procedure was carried out as follows: 10 mg of GIF-4 was added to 10 mL of a 1000 ppm $[AuBr_4]^-$ solution (pH adjusted to 3.8). The mixture was stirred continuously for 12 hours at room temperature. Subsequently, the solid was separated from the liquid phase via centrifugation and filtration. The concentration of gold in the resulting solution was then analysed with ICP-OES.

Selectivity in competing cations.

To evaluate cation selectivity, 20 mg of GIF-4 was added to 10 mL of a mixed-metal ion solution containing 20 ppm Au(III) and 100 ppm of each competing cation. The mixture was stirred for 6 hours at room temperature. Subsequently, the solid was separated by centrifugation, and the supernatant was filtered through a 0.22 μm membrane filter. The concentrations of Au and all competing cations in the filtrate were then determined separately via ICP-OES.

Selectivity in competing cations.

To evaluate anion selectivity, 50 mg of GIF-4 was added to 10 mL of an Au(III) solution (20 ppm) containing competing anions (Cl^-, NO_3^-, SO_4^{2-}) at concentrations ranging from 50- to 1000-fold molar excess relative to Au(III). The mixture was stirred for 6 hours at room temperature. Subsequently, the solid was separated by centrifugation, and the supernatant was filtered through a 0.22 μm membrane filter. The concentrations of Au and all competing cations in the filtrate were then determined separately via ICP-OES.

The regeneration efficiency and cycling stability.

The regeneration efficiency and cycling stability of GIF-4 material were evaluated through sequential adsorption-desorption cycles. In each cycle, 50 mg of GIF-4 was dispersed in 10 mL of a 20 ppm Au(III) solution and stirred for 30 min at room temperature to achieve adsorption equilibrium. The loaded material was then separated via centrifugation and transferred into 20 mL of a stripping agent composed of 0.2 M HCl and 0.2 M thiourea, where it was stirred for 12 h at room temperature to desorb the gold. Following desorption, the regenerated GIF-4 was centrifuged and washed thoroughly: first three times with deionized water, then soaked in THF for 6 h, and finally rinsed twice again with deionized water. After washing, the material was dried under vacuum at 60°C for 12 h before being reused in the next adsorption cycle. This process was repeated over five cycles to assess the material's recovery performance.

NBS/H_2O solution for gold leaching.

Gold can be efficiently leached from SIM cards using the following procedure: a defined quantity of SIM cards (e.g., 50 chips) is immersed in 100 mL of an aqueous NBS solution (0.084 M). The pH is adjusted to between 2 and 4, and the mixture is stirred at room temperature for 2–5 min. Once the leaching is complete, the processed cards are removed, and a new batch of SIM cards can be introduced to repeat the cycle. In the last run, an excess of sodium thiosulfate was added to remove the Br_2, and the pH was adjusted to 3.8 for the following adsorption experiment.

Extraction of gold from e-waste leachate with GIF-4.

1.0 g of GIF-4 was added to the gold-containing NBS/H_2O leaching solution. The pH of the mixture was adjusted to ca. 3.8, followed by stirring at room temperature for 6 h. Finally, the concentration of Au, Cu, and Ni in the solution was measured to determine the removal efficiency.

Leaching SIM cards with aqua regia.

Ten SIM cards were placed in a 250 mL flask, to which 15 mL of aqua regia ($HCl:HNO_3$ = 3:1, v/v) was added. The mixture was stirred for 1 hour at room temperature. Subsequently, the solution was diluted to a total volume of 100 mL with deionized water. After initial filtration through filter paper, the leachate was further filtered using a 0.22 μm membrane filter prior to the quantification of Au, Cu, and Ni concentrations via ICP-MS/AAS.

Figure S1. Photograph of the planetary ball mill

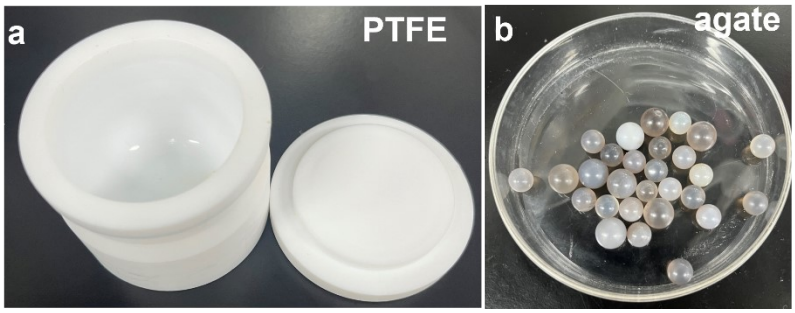

Figure S2. (a) 100 mL PTFE jar with the (b) agate balls

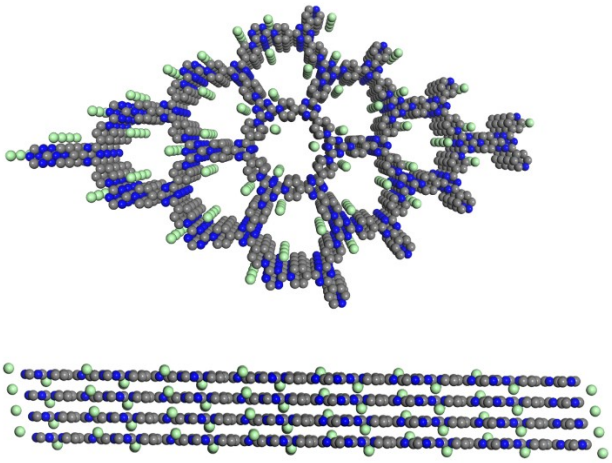

Figure S3. Simulated AA configuration of GIF-4.

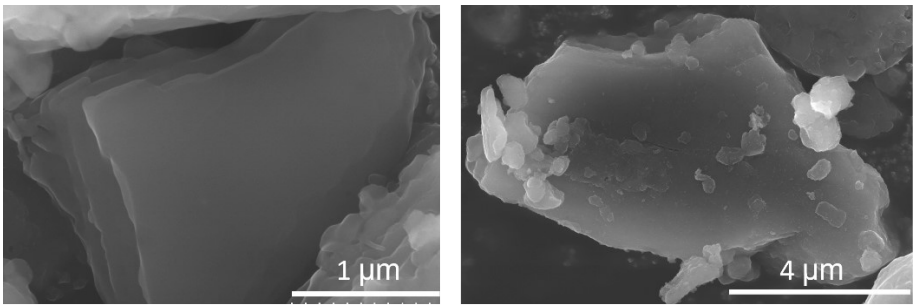

Figure S4 SEM images of GIF-4 showing the layered structure.

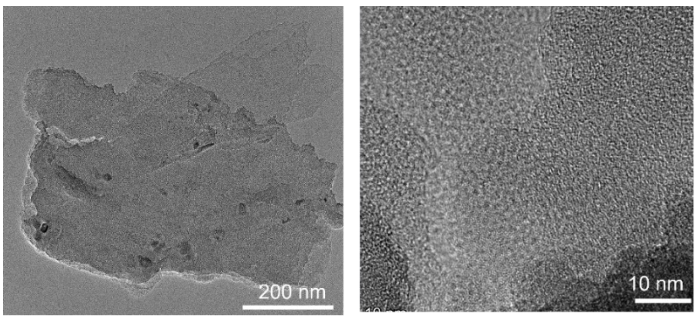

Figure S5 TEM images of GIF-4.

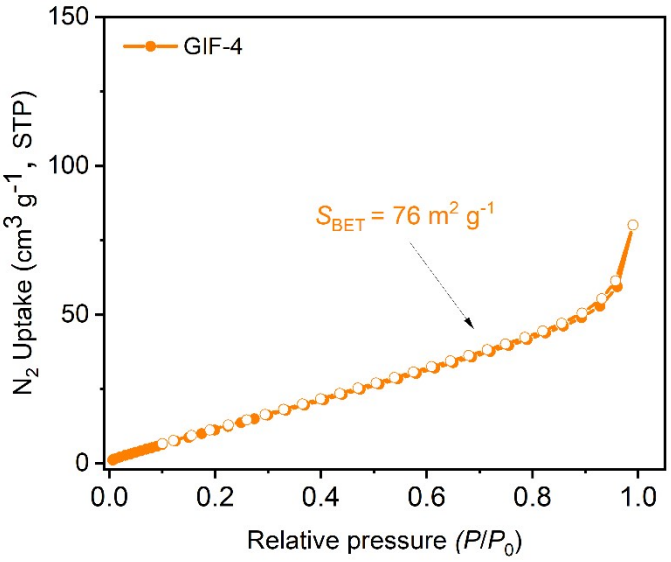

Figure S6. Nitrogen adsorption isotherm for the analysis of porous structure.

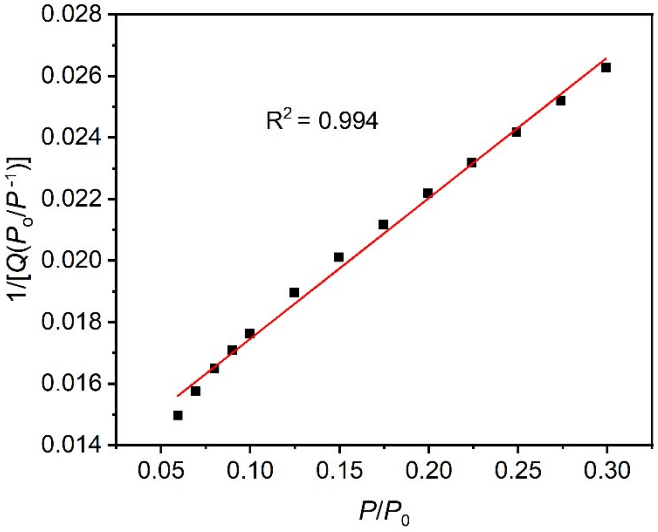

Figure S7. Curve for the calculation of the BET specific surface area.

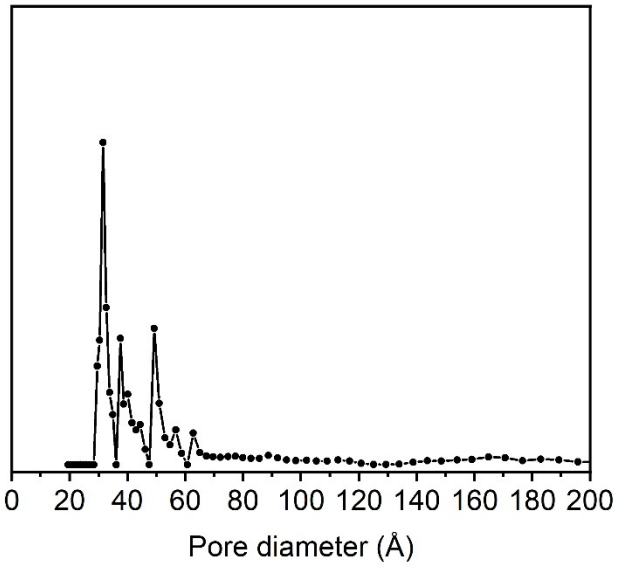

Figure S8. Pore size distribution of GIF-4.

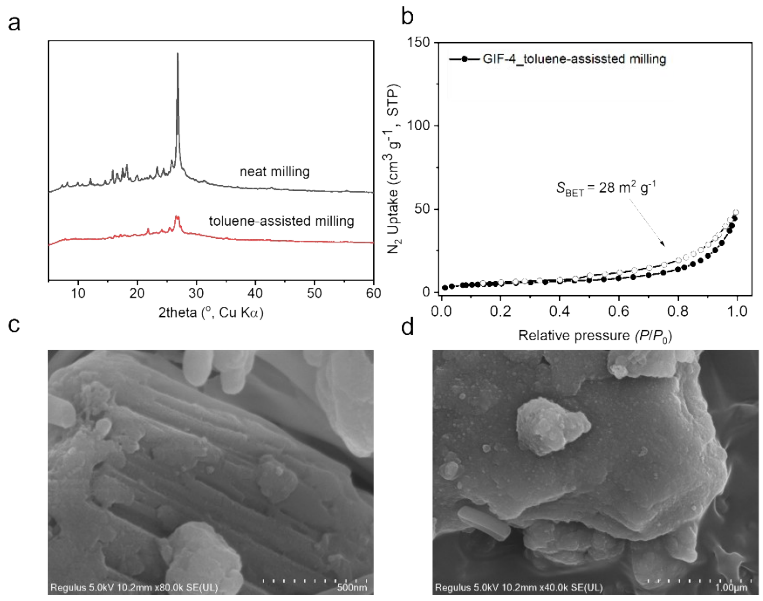

Figure S9. Characterization of GIF-4 synthesized via toluene-assisted grinding. (a) XRD patterns comparing neat-milling (black) and toluene-assisted milling (red) samples. (b) N_2 adsorption-desorption isotherm (77 K) of GIF-4 prepared by toluene-assisted milling. (c, d) SEM images illustrating the morphology of the toluene-assisted milled GIF-4.

Table S1. Elemental analysis of GIF-4.

Item	C (wt%)	H (wt%)	N (wt%)	C/N
Calculated	50.6	2.83	25.2	2.0
Experimental	55.3	4.4	24.3	2.3

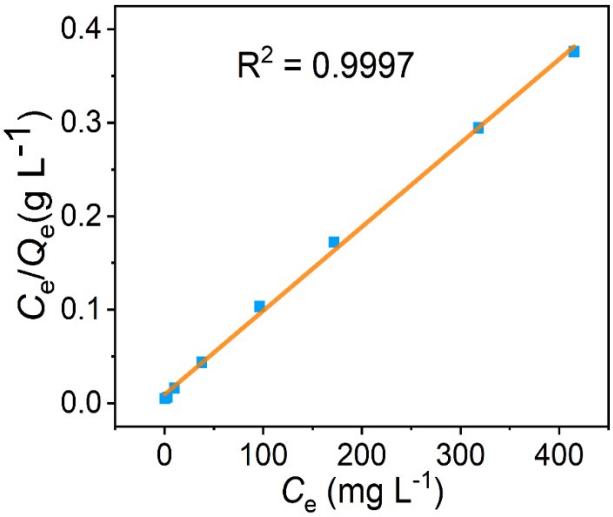

Figure S10. Fitting of the linear Langmuir model**.**

Table S2. Parameters of the Langmuir model fitting.

Parameters	Values
Q_m	1110.2 mg
K_L	0.32 L/mg
R^2	0.9997

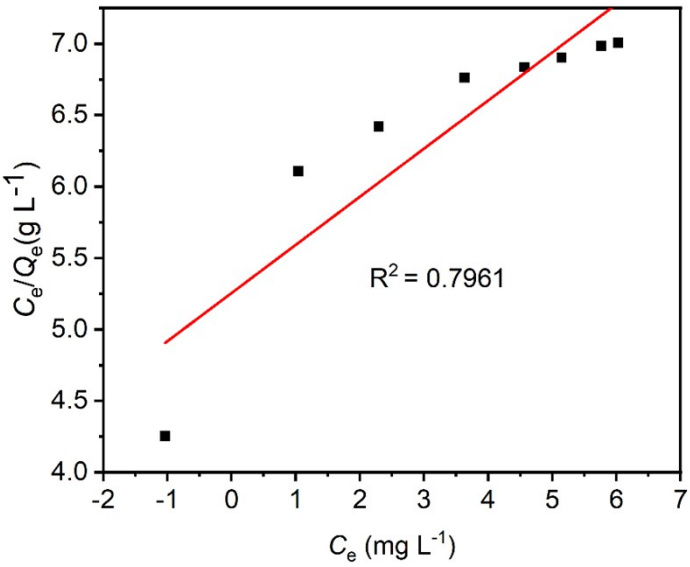

Figure S11. Fitting of the linear Freundlich model**.**

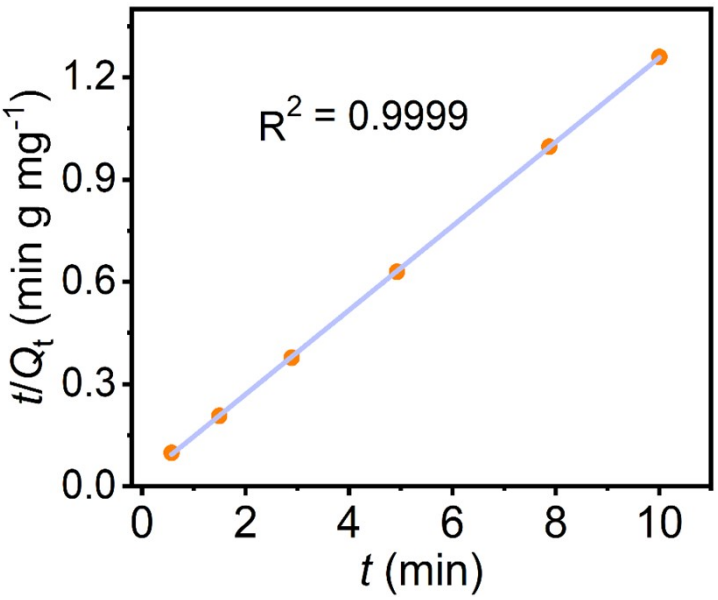

Figure S12. Fitting of the linear PSO model.

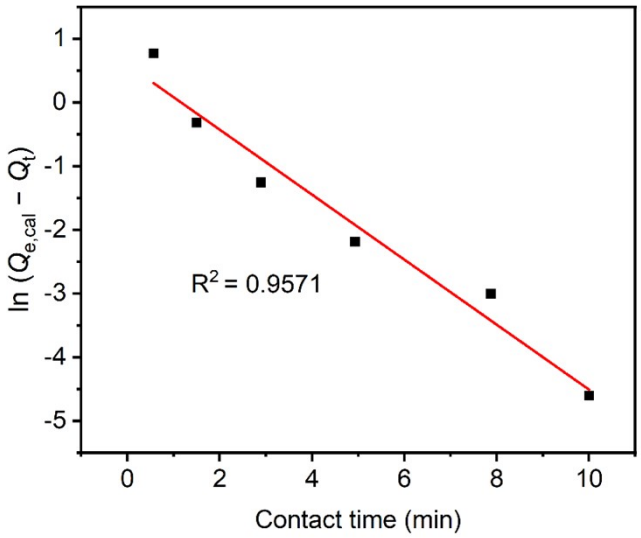

Figure S13. Fitting of the linear Pseudo-First-Order model.

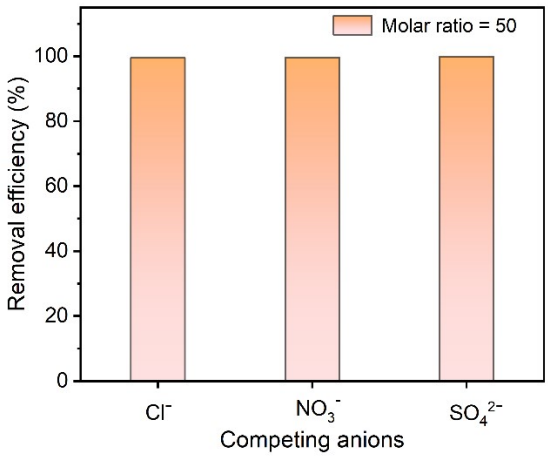

Figure S14. Anion selectivity measured with a 50-fold molar excess of competing ions.

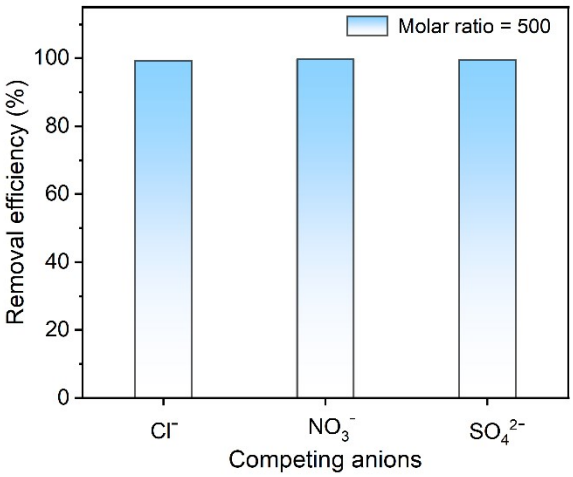

Figure S15. Anion selectivity measured with a 500-fold molar excess of competing ions.

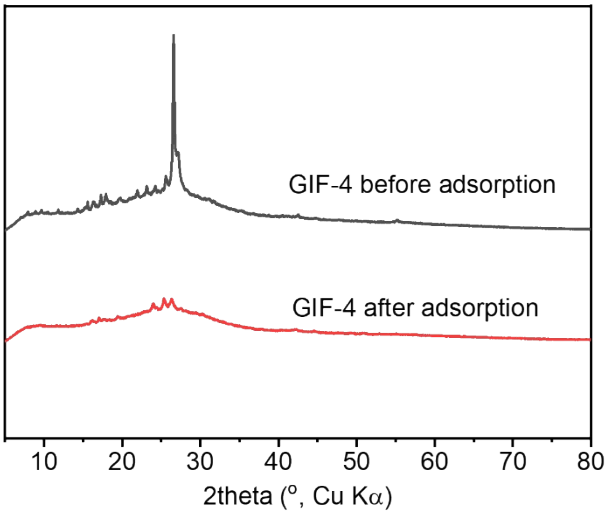

Figure S16. PXRD patterns of GIF-4 before (black) and after (red) gold adsorption.

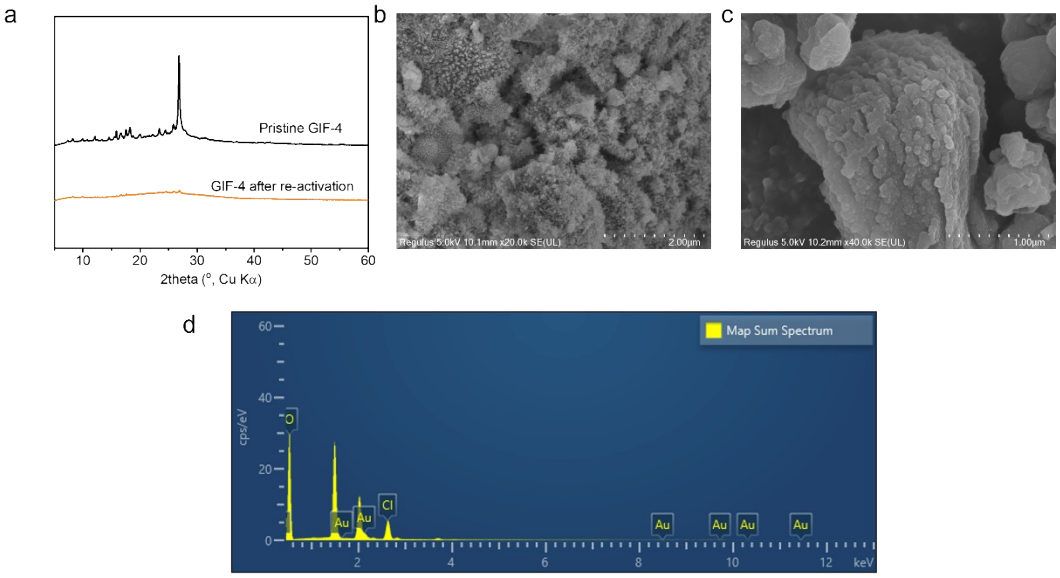

Figure S17. Characterization of the reactivated GIF-4 material after gold desorption: (a) PXRD pattern showing no characteristic peaks of metallic gold; (b, c) SEM image revealing morphological changes; (d) EDS spectrum indicating residual trace gold.

Table S3. Comparison of Au(III) adsorption performance between ionic/functionalized COFs/MOFs.

Material	Type	Q_{max} ($mg \cdot g^{-1}$)	Equilibrium Time	Selectivity / Features	Synthesis Conditions	Refs
UiO-67-MAA	Defective MOF	2253.2	10 min	High selective recovery from wastewater	One-step solvent method, 120 °C, 24 h	1
Ionic-nano-COFA	Amide-linked Ionic nano-COF	1334	Fast	Stable in acidic E-waste	Solvothermal, 120 °C, 3 days	2
im-PYTA-PZDH-COF	Imidazopyridinium-linked COF	1558	10 min	95% uptake in 10 min	Solvothermal, 120 °C, 3 days	3
TpTGCl (Nanopaper)	Guanidinium-based COF	1794	Fast	High efficiency in CPU leaching	Solvothermal, 120 °C, 3 days	4
Imi-PPOPs-Br	Cationic Porphyrin POP	1543	Fast	Specific to $AuCl_4^-$	Bottom-up synthesis, 180 °C, 72 h	5
V-PPOP-Br	Viologen-linked Cationic POP	1103	N/A	High selectivity	Solvothermal, 120 °C, 72 h	6
UiO-66-SPA	Carboxypyridine-func. MOF	1004	40 min	2.65x higher than non-func. UiO-66	Post-synthetic modification, 80 °C, 12 h	7
Fe-BTC/PPPDA	MOF/Polymer Composite	934	~2 min	Selective trace extraction	In situ polymerization, 70 °C	8
Zr-MOF (Piperazine)	Piperazine-based MOF	900	N/A	High stability in acidic media	Solvothermal, 120 °C	9
DUT-67-TMA	Thiophene-func. MOF on Fabric	586	60 min	Passive sampling & recovery	Solvothermal, 120 °C, 24 h	10
GIF-4	**Pyridium**	**1110**	**10 min**	**Highly selective for $AuCl_4^-$ over competing anions**	**Mechanochemical synthesis, 2h**	**This work**

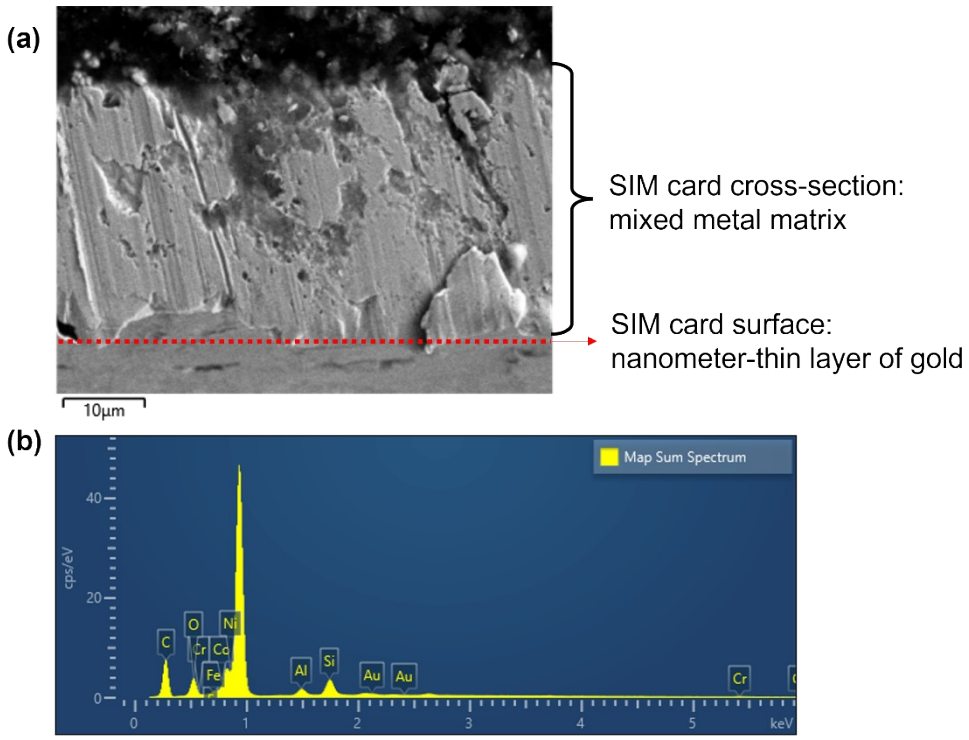

Figure S18. (a) SEM image of the cross-section of the SIM card chips, (b) the corresponding EDS analysis of the cross-section of SIM card.

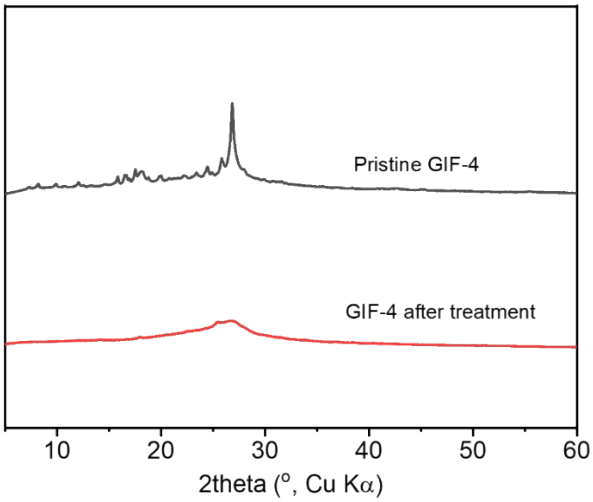

Figure S19. PXRD comparison of GIF-4 after treatment with NBS/H_2O leachate.

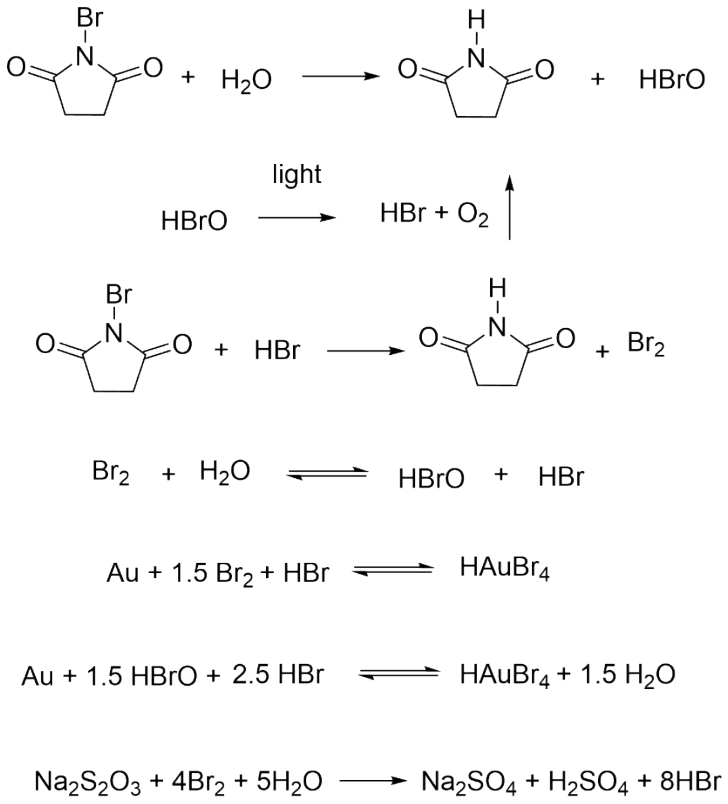

Figure S20. Proposed reaction mechanisms of gold leaching with NBS in aqueous solution[11-13].

Table S4. ABC classification criteria for the Biwer–Heinzle environmental assessment method.

Impact Group (IG)	Impact Category (IC)	Input (I)/Output(O)	Class A (high concern)	Class B (medium concern)	Class C (low/negligible concern)
Resources	Raw Material Availability	I	Only fossil-based; predicted exhaustion within 30 years	Only fossil-based; predicted exhaustion in 30–100 years	Renewable, or guaranteed supply >100 years
Grey Inputs	Complexity of Synthesis	I	>10 synthesis steps	3–10 synthesis steps	<3 synthesis steps
Grey Inputs	Critical Materials Used	I	Critical materials (heavy metals, AOX, PCB) used or	Critical materials involved in	No critical compounds

			produced in stoichiometric amounts.	substoichiometric amounts	involved
Organisms	Acute Toxicity	I/O	EU T^{+}; R26–28,32,50; LD_{50} oral <25 mg/kg; LC_{50} inh <200 mg/m³	EU T, Xn, Xi; LD_{50} oral 25–200 mg/kg; LC_{50} inh 200–2000 mg/m³	No acute toxicity; LD_{50} oral >200 mg/kg; LC_{50} inh >2000 mg/m³
Organisms	Chronic Toxicity	I/O	MAK <1 mg/m³; IARC 1,2A; R45–49,60,61	MAK 1–10 mg/m³; IARC 2B,3; R33,40,62,63	MAK >10 mg/m³; IARC 4
Organisms	Endocrine Disruption Potential	I/O	— (not defined)	Scientifically proved or suspected endocrine effect	No known hormonal effect
Component Risk	Thermal Risk (flammability/reactivity)	I/O	Flash point <38 °C; or explosive; NFPA F+R 3–4	Flash point 38–100 °C; NFPA F+R 2	Flash point >100 °C; stable; NFPA F+R 0–1
Air	Global Warming Potential (GWP)	O	GWP >20	GWP <20	No GWP
Air	Ozone Depletion Potential (ODP)	O	ODP >0.5	ODP <0.5	No ODP
Air	Acidification Potential (AP)	O	AP >0.5	AP <0.5	No AP
Air	Photochemical Ozone Creation Potential (POCP)	O	POCP >30 or NOx	2 < POCP <30	POCP <2 or no effect known
Air	Odour	O	— (not defined)	Odour threshold <300 mg/m³	Odour threshold >300 mg/m³ or no odour
Water/Soil	Eutrophication Potential (EP)	O	N-content >0.2 **or** P-content >0.05 (mass fraction)	N-content <0.2 **and** P-content <0.05	Contains neither N nor P
Water/Soil	Organic Carbon Pollution Potential (OCPP)	O	— (not defined)	ThOD or COD >0.2 g O_2/g substrate	ThOD and COD <0.2 g O_2/g substrate; or non-organic

Table S5. Biwer-Heinzle method[14] for input environmental evaluation.

Component	CAS No.	Role	Resources	Grey Inputs	Organisms	Component Risk	EF_MW	EF_Mult	MI (kg/kg Au)*	EI_MW	EI_Mult
SIM Cards	N/A	Gold source	**B**	**C**	**C**	**C**	0.08	1.3	372	29.8	484
NBS	128-08-5	Oxidant precursor	B	B	B	B	0.30	2.86	0.124	0.037	0.355
HBr	10035-10-6	Complexing agent	B	C	A	C	0.33	5.2	0.093	0.031	0.484
Br_2	7726-95-6	Active oxidant	B	C	A	A	0.58	20.8	0.111	0.064	2.31
$Na_2S_2O_3$	7772-98-7	Quenching agent	B	C	C	C	0.08	1.3	0.027	0.002	0.035
TCT	108-77-0	GIF-4 precursor 1	B	B	A	A	0.58	20.8	1.06	0.615	22.0
TPT	42333-78-8	GIF-4 precursor 2	B	B	B	B	0.30	2.86	1.80	0.540	5.15
TOTAL INPUT									**375**	**31.1**	**514**

Table S6. Biwer-Heinzle method[14] for output environmental evaluation.

Component	CAS No.	Role	Air	Water/Soil	Organisms	Component Risk	EF_MW	EF_Mult	MI (kg/kg Au)*	EI_MW	EI_Mult
$HAuBr_4$	37088-67-8	Target product	C	B	A	C	0.33	5.2	0.240	0.079	1.25
GIF-4	N/A	Adsorption carrier	C	C	C	C	0	1.0	2.86	0	2.86
Na_2SO_4	7757-82-6	Byproduct	C	C	C	C	0	1.0	0.025	0	0.025
HBr	1003	Residual	C	C	A	CC	0.25	4.0	0.10	0.026	0.412

	5-10-6	Br-species							3		
Succinimide	123-56-8	Byproduct	C	B	B	C	0.15	1.69	0.069	0.010	0.117
H_2O	7732-18-5	Byproduct	C	C	C	C	0	1.0	0.013	0	0.013
TOTAL OUTPUT									**3.31**	**0.115**	**4.68**

Table S7. Complete mass balance summary

Component	Role	Mass (g)	MI (kg/kg Au)	EF_Mult	EI_Mult
Inputs					
SIM Cards	Gold source	20.5	372	1.3	484
NBS	Oxidant precursor	0.0068	0.124	2.86	0.355
HBr	Complexing agent	0.0051	0.093	5.2	0.484
Br_2	Active oxidant	0.0061	0.111	20.8	2.31
$Na_2S_2O_3$	Quenching agent	0.0015	0.027	1.3	0.035
TCT	GIF-4 precursor 1	0.0586	1.06	20.8	22.0
TPT	GIF-4 precursor 2	0.0992	1.80	2.86	5.15
Total Input		**20.677**	**375**	—	**514**
Outputs					
$HAuBr_4$	Target product	0.0132	0.240	5.2	1.25
GIF-4	Adsorption carrier	0.1578	2.86	1.0	2.86
Na_2SO_4	Byproduct	0.0014	0.025	1.0	0.025
HBr	Residual Br-species	0.0057	0.103	4.0	0.412
Succinimide	Byproduct	0.0038	0.069	1.69	0.117
H_2O	Byproduct	0.0007	0.013	1.0	0.013
Total Output		**0.1826**	**3.31**	—	**4.68**

Tables S8. Final GEI calculation

Parameter	Input	Output
MI_Process	375	3.31
EI_Process (EF_MW)	31.1	0.115
GEI_MW = EI/MI	**0.083**	**0.035**
EI_Process (EF_Mult)	514	4.68
GEI_Mult = EI/MI	**1.37**	**1.41**

Table S9. Comparison of GEI values for different extraction methods

Process	GEI_MW (Input)	GEI_MW (Output)	GEI_Mult (Input)	GEI_Mult (Output)
This work	**0.083**	**0.035**	**1.37**	**1.41**
Chlorination	0.05	0.07	1.58	1.59
Cyanidation	0.10	0.13	2.21	2.68
Aqua regia	0.29	0.41	8.67	31.19

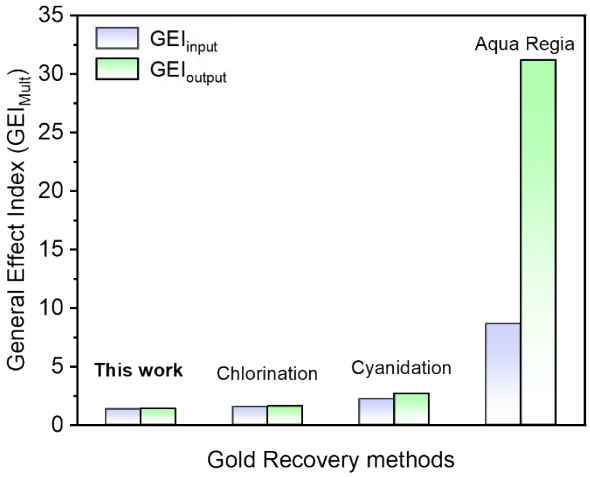

Figure S21. Comparison of quantitative environmental index GEI_{Mult} using the Biwer-Heinzle method.

Table S10. The atomic coordinate of GIF-4 with AA mode after Pawley refinement.

GIF-4, AA stacking			
Triclinic, *P*1			
a = 14.5848 Å, b = 14.5836 Å, c = 3.5829Å			
α = 88.1933°, β =106.4870°, γ = 119.9959°			
Atom	**x**	**y**	**z**
N1	N	1.12028	-6.13625
C2	C	1.066	-6.24384
N3	N	1.12031	-6.29712
C4	C	1.22796	-6.24386
N5	N	1.28129	-6.1362
C6	C	1.22795	-6.08185
N7	N	1.28464	-6.30086
C8	C	1.22844	-6.40958
C9	C	1.28201	-6.46636
C10	C	1.39449	-6.41119
C11	C	1.45095	-6.29982
C12	C	1.39439	-6.24599
C13	C	1.45268	-6.46956
N14	N	1.39915	-6.57718
C15	C	1.45273	-6.63129
N16	N	1.56055	-6.57698
C17	C	1.61474	-6.46943
N18	N	1.56048	-6.41611
C19	C	1.39454	-6.74786
C20	C	1.73154	-6.41105
C21	C	1.78814	-6.46541
C22	C	1.89879	-6.40864
N23	N	1.95224	-6.30072
C24	C	1.89809	-6.2466
C25	C	1.78743	-6.30045
C26	C	1.28201	-6.80486

C27	C	1.22844	-6.91524
N28	N	1.28467	-6.96812
C29	C	1.39447	-6.91355
C30	C	1.45104	-6.80313
Cl31	Cl	0.01639	0.97266
Cl32	Cl	1.01898	0.50608
Cl33	Cl	0.4881	0.96511

Table S11. The atomic coordinate of GIF-4 with AB mode after Pawley refinement.

GIF-4, AB stacking			
Triclinic, *P*1			
a = 14.6811Å, b = 14.6895Å, c = 7.2386Å			
α = 87.8815°, β = 106.9264°, γ = 119.9600°			
Atom	**x**	**y**	**z**
N1	0.17483	0.90441	0.67842
C2	0.12082	0.79767	0.67928
N3	0.17486	0.74468	0.68032
C4	0.28196	0.7974	0.68164
N5	0.33502	0.90422	0.68186
C6	0.28196	0.95826	0.67985
N7	0.33835	0.74071	0.68181
C8	0.28244	0.63284	0.67032
C9	0.33574	0.57638	0.6706
C10	0.44765	0.63098	0.6827
C11	0.50382	0.74149	0.69417
C12	0.44754	0.79503	0.69342
C13	0.50554	0.57294	0.68354
N14	0.45228	0.46615	0.68277
C15	0.50558	0.41234	0.68556
N16	0.61286	0.46611	0.68828
C17	0.66678	0.57281	0.68792
N18	0.61279	0.62585	0.68614

C19	0.4477	0.29668	0.68666
C20	0.78297	0.63061	0.6901
C21	0.83929	0.57654	0.69412
C22	0.94938	0.63275	0.69634
N23	1.00255	0.73982	0.6942
C24	0.94868	0.79365	0.69063
C25	0.83858	0.74034	0.68831
C26	0.33574	0.24026	0.67429
C27	0.28244	0.13073	0.67585
N28	0.33838	0.07814	0.68931
C29	0.44762	0.13215	0.70126
C30	0.50391	0.24171	0.70023
N31	0.80341	1.18965	1.21604
C32	0.7494	1.08291	1.21689
N33	0.80344	1.02992	1.21794
C34	0.91054	1.08264	1.21926
N35	0.9636	1.18946	1.21947
C36	0.91054	1.2435	1.21747
N37	0.96693	1.02595	1.21943
C38	0.91102	0.91809	1.20794
C39	0.96431	0.86162	1.20822
C40	1.07622	0.91622	1.22032
C41	1.1324	1.02673	1.23178
C42	1.07612	1.08027	1.23103
C43	1.13412	0.85818	1.22116
N44	1.08086	0.75139	1.22039
C45	1.13416	0.69758	1.22317
N46	1.24144	0.75135	1.22589
C47	1.29535	0.85805	1.22553
N48	1.24137	0.91109	1.22376
C49	1.07627	0.58192	1.22428
C50	1.41155	0.91585	1.22771

C51	1.46787	0.86178	1.23174
C52	1.57796	0.91799	1.23395
N53	1.63113	1.02506	1.23182
C54	1.57726	1.07889	1.22825
C55	1.46716	1.02558	1.22593
C56	0.96432	0.5255	1.21191
C57	0.91102	0.41597	1.21346
N58	0.96696	0.36338	1.22693
C59	1.0762	0.41739	1.23888
C60	1.13249	0.52695	1.23785
Cl61	0.36937	0.16908	0.21504
Cl62	0.83483	0.62834	0.27024
Cl63	0.36595	0.62734	0.19679
Cl64	0.70673	-0.16821	0.75752
Cl65	0.76498	0.35176	0.69711
Cl66	1.25132	0.34411	0.78705

Reference

(1) Wang, Z.; Bao, Z.; Wang, X.; Xia, C.; Xu, D.; Wang, S.; Li, W. Regulator-induced defective functionalization of MOFs: Efficient recovery of gold ions from wastewater. *Journal of Materials Science & Technology* **2026**, *247*, 302-311.

(2) Xiong, C.; Wang, Y.; Liang, K.; Wu, C.; Wu, W.; Chen, Q. Ionic Nanocovalent Organic Frameworks for Enhanced Gold Recovery from Electronic Wastewater. *ChemSusChem* **2025**, *18* (22), e202501155.

(3) Yang, X.; Jiang, D.; Cheng, Y.; Fu, Y.; Li, X.; Liu, G.; Ding, X.; Han, B. H.; Xu, Q.; Zeng, G. Imidazopyridinium-Linked Covalent Organic Frameworks for Efficient Gold Recovery. *Small Methods* **2024**, *9* (7).

(4) Xu, Q.; Du, X.-H.; Luo, D.; Strømme, M.; Zhang, Q.-F.; Xu, C. Gold recovery from E-waste using freestanding nanopapers of cellulose and ionic covalent organic frameworks. *Chemical Engineering Journal* **2023**, *458*.

(5) Ding, R.; Liu, J.; Wang, T.; Zhang, X. Bottom-up synthesis of cationic porphyrin-based porous organic polymers for highly efficient and selective recovery of gold. *Chemical Engineering Journal* **2022**, *449*.

(6) Chen, Y.; Li, Z.; Ding, R.; Liu, T.; Zhao, H.; Zhang, X. Construction of porphyrin and

viologen-linked cationic porous organic polymer for efficient and selective gold recovery. *J Hazard Mater* **2022**, *426*, 128073.

(7) Wang, X.; Wang, Z.; Xia, C.; Bao, Z.; Xu, D.; Ma, Y.; Wang, S.; Li, W. Carboxypyridine-Functionalized MOFs for Enhanced Au(III) Recovery. *Applied Organometallic Chemistry* **2025**, *39* (9).

(8) Sun, D. T.; Gasilova, N.; Yang, S.; Oveisi, E.; Queen, W. L. Rapid, Selective Extraction of Trace Amounts of Gold from Complex Water Mixtures with a Metal–Organic Framework (MOF)/Polymer Composite. *Journal of the American Chemical Society* **2018**, *140* (48), 16697-16703.

(9) Meoli, M.; Roth, J.; Stoian, D. C.; Belin, A. F. S.; Scopelliti, R.; Queen, W. L. Stable Zirconium-Piperazine Metal–Organic Frameworks for Efficient Gold Recovery. *Chemistry of Materials* **2026**, *38* (6), 2767-2777.

(10) Gouma, V.; Makri, E. C.; Andreou, E. K.; Buchsteiner, E.; Armatas, G. S.; Manos, M. J.; Giokas, D. L. An Amino-Thiophene Functionalized Metal-Organic Framework on Fabric for Selective Extraction, Recovery, and Passive Sampling of Gold Ions and Nanoparticles. *Chem Mater* **2025**, *37* (18), 7147-7158.

(11) Senanayake, G. Gold leaching in non-cyanide lixiviant systems: critical issues on fundamentals and applications. *Minerals Engineering* **2004**, *17* (6), 785-801.

(12) Yue, C.; Sun, H.; Liu, W.-J.; Guan, B.; Deng, X.; Zhang, X.; Yang, P. Environmentally Benign, Rapid, and Selective Extraction of Gold from Ores and Waste Electronic Materials. *Angewandte Chemie International Edition* **2017**, *56* (32), 9331-9335.

(13) Kim, E.-y.; Kim, M.-s.; Lee, J.-c.; Pandey, B. Selective recovery of gold from waste mobile phone PCBs by hydrometallurgical process. *Journal of hazardous materials* **2011**, *198*, 206-215.

(14) Wang, J.; Lu, Y.; Xu, Z. Identifying Extraction Technology of Gold from Solid Waste in Terms of Environmental Friendliness. *ACS Sustainable Chemistry & Engineering* **2019**, *7* (7), 7260-7267.